Journal of Geodesy (2001) 75: 216–226

Journal of Geodesy

Quasi-stationary sea surface topography estimation by the multiple input/output method

V. D. Andritsanos[1] (✉), M. G. Sideris[2], I. N. Tziavos[1]

[1] Department of Geodesy and Surveying, Aristotle University of Thessaloniki, University Box 440, 540 06 Thessaloniki, Greece
[2] Department of Geomatics Engineering, University of Calgary, 2500 University Drive N.W., Calgary, Alberta, T2N 1N4 Canada

Received: 19 October 1999 / Accepted: 23 October 2000

Abstract. Multiple input/multiple output system theory (MIMOST) is briefly presented, and the application of the method to the quasi-stationary sea surface topography (QSST) estimation and the filtering of the input observations are discussed. The repeat character of satellite altimetry missions provides more than one sample of the measured sea surface height (SSH) field, and an approximation of the input signal and error power spectral densities can be determined using this successive information. A case study in the Labrador Sea is considered using SSHs from ERS1 phases C and G, ERS1-GM, ERS2 phase A and TOPEX/POSEIDON altimetric missions in combination with shipborne gravity anomalies. The time period of the observations in this study is from 1993 to 1998. Some comparisons between the techniques used for the power spectral density approximation are carried out and some remarks on the properties of the estimated QSST are presented.

Key words: Multiple Input/Multiple Output Method – Satellite Altimetry – Sea Surface Topography – Geoid – Gravity

1 Introduction

The use of spectral methods in physical geodesy has been developed during recent decades. The basic advantage of the analysis in the spectral domain is the algebraic simplicity of the convolution integrals. As is well known, the convolution integrals are transformed to multiplications in the spectral domain and the evaluation of some complicated formulas in gravity field modeling is speeded up.

The heterogeneous data combination and the appropriate error propagation using spectral methods are presented in Sideris (1996). The input/output system theory (IOST) is based on the analysis given by Bendat and Piersol (1986) and the proper adaptation in gravity field applications is discussed in Sideris (1996). Gravity field applications of IOST can be found in Li (1996) and Tziavos et al. (1996a, b, c, 1998) and an application to airborne gravimetry was presented by Wu and Sideris (1995). The similarities and the differences between IOST and least-squares (LS) collocation were analyzed by Sansò and Sideris (1997). The multiple input/multiple output system theory (MIMOST) has recently been used by Andritsanos and Tziavos (1999) and Andritsanos et al. (1999). In these papers, some simulation studies were performed in the Labrador Sea using Gaussian noises for the input gravity and geoid data filtering, as well as for the quasi-stationary sea surface topography (QSST) estimation.

Many researchers developed appropriate algorithms for an accurate estimation of the sea surface topography (SST). Engelis (1983) presented a global solution based on harmonic analysis using SEASAT altimeter data. A comparable solution was presented by Tai and Wunsch (1984) using filtered SEASAT data to reduce aliasing. A global solution based on harmonic analysis of pure oceanographic data from Levitus (1982) was computed by Engelis (1987b). In another approach, a simultaneous radial orbit error reduction was achieved (Engelis, 1987a). SEASAT altimeter data were also used in the SST estimation presented by Engelis and Knudesn (1989). Knudsen (1991) estimated the QSST in the Faeroe Islands, as well as the time-variant part with (LS) collocation, and constructed error covariances using information from previous studies and Butterworth filters for the analytical expressions. Hwang (1995) estimated a global SST solution based on orthonormal functions for GEOSAT. Rapp et al. (1996) recommended the use of spherical harmonics for SST representation, followed by transformation to the orthonormal basis. Sanchez et al. (1997) implemented the height function representation, introduced by Rao et al. (1987), and compared it with spherical harmonics. Recently, Pavlis et al. (1998) presented a global estimation of the SST based on spherical harmonics and an eigenvalue analysis of the Proudman functions.

In the present paper, a QSST estimation procedure based on MIMOST is presented. A 6 year time period is chosen in order to verify the quasi-stationary character of the approximation. Precomputed input error and signal information are used for the sea surface height (SSH) observations based on a successive track analysis. Two slightly different methods are applied for determining the input error power spectral density (PSD) and the resulting two-dimensional (2-D) covariances are compared with each other. The PSDs/covariances are calculated for each separate year and each specific satellite, and are introduced into the MIMOST procedure for the QSST estimation.

2 Theoretical background

2.1 MIMOS theory

A multiple input/multiple output system (MIMOS) is presented in Fig. 1, where y_{io} are the input observations, y_i are the pure input signals, m_i are the input noises, h_{io} are the unknown transfer functions that filter out the input noise, x_j are the unknown output signals, and e_j are the output noises. The total number of input data i may be equal to or different than the number of output signals j. The interaction between every input and output is also presented in Fig. 1.

The aim of the method is the determination of the impulse response functions h_{io} based on some criterion. The minimization criterion of the output error PSD is used for the transfer function estimation; see, for example, Bendat and Piersol (1986) and Sideris (1996). If matrix notations are applied for the description of the system depicted in Fig. 1, then the following equations are valid; see, for example, Bendat and Piersol (1986), Sideris (1996), Andritsanos and Tziavos (1999), and Andritsanos et al. 1999:

$$\mathbf{Y_o} = \begin{bmatrix} Y_1 + M_1 \\ Y_2 + M_2 \\ \vdots \\ Y_q + M_q \end{bmatrix}, \quad \mathbf{X_o} = \begin{bmatrix} X_1 - E_1 \\ X_2 - E_2 \\ \vdots \\ X_w - E_w \end{bmatrix} \tag{1}$$

where capital letters stand for the spectra of the respective quantities and the output error matrix is given as follows:

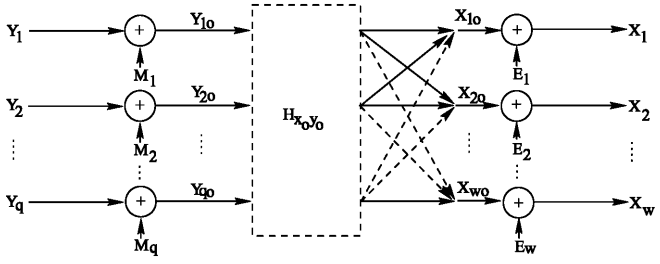

Fig. 1. Multiple-input/multiple-output system

$$\mathbf{E} = \mathbf{X} - \mathbf{X_o} = \mathbf{X} - \mathbf{H}_{\mathbf{x_o y_o}}(\mathbf{Y} + \mathbf{M}) \tag{2}$$

The transfer function matrix is of the form:

$$\mathbf{H}_{\mathbf{x_o y_o}} = \begin{bmatrix} H_{x_{1o}y_{1o}} & H_{x_{1o}y_{2o}} & \cdots & H_{x_{1o}y_{qo}} \\ H_{x_{2o}y_{1o}} & H_{x_{2o}y_{2o}} & \cdots & H_{x_{2o}y_{qo}} \\ \vdots & \vdots & \ddots & \vdots \\ H_{x_{wo}y_{1o}} & H_{x_{wo}y_{2o}} & \cdots & H_{x_{wo}y_{qo}} \end{bmatrix} \tag{3}$$

which shows the dependence of each output on the inputs. If Eq. (2) is multiplied by its complex conjugate form, an estimation of the output error PSD can be computed following the periodogram approach as described in Marple (1987) and Bendat and Piersol (1986)

$$\mathbf{P_{ee}} = \mathbf{P_{xx}} - \mathbf{H}_{\mathbf{x_o y_o}}\mathbf{P}_{\mathbf{y_o x}} - \mathbf{P}_{\mathbf{x y_o}}\mathbf{H}^{*}_{\mathbf{y_o x_o}} + \mathbf{H}_{\mathbf{x_o y_o}}\mathbf{P}_{\mathbf{y_o y_o}}\mathbf{H}^{*}_{\mathbf{y_o x_o}} \tag{4}$$

where the asterisk stands for the complex conjugate of the matrix elements. The optimal transfer functions can be calculated by the minimization of the output error PSD matrix $\mathbf{P_{ee}}$ as follows:

$$\frac{\partial \mathbf{P_{ee}}}{\partial \mathbf{H}^{*}_{\mathbf{y_o x_o}}} = 0 \tag{5}$$

$$\Rightarrow -\mathbf{P}_{\mathbf{x y_o}} + \mathbf{H}_{\mathbf{x_o y_o}}\mathbf{P}_{\mathbf{y_o y_o}} = 0 \tag{6}$$

Assuming no correlation between input signals and input noises, the optimal transfer function matrix is

$$\mathbf{H}_{\mathbf{x_o y_o}} = \mathbf{P}_{\mathbf{x y}}\mathbf{P}^{-1}_{\mathbf{y_o y_o}} = \mathbf{P}_{\mathbf{x y}}(\mathbf{P_{yy}} + \mathbf{P_{mm}})^{-1} \tag{7}$$

Then the output signal vector and the output noise PSD matrices are

$$\mathbf{X_o} = \mathbf{H}_{\mathbf{x_o y_o}}\mathbf{Y_o} = \mathbf{P}_{\mathbf{x y}}(\mathbf{P_{yy}} + \mathbf{P_{mm}})^{-1}(\mathbf{Y} + \mathbf{M}) \tag{8}$$

The similarities between MIMOST and least-squares collocation (LSC), as presented in Sansò and Sideris (1997), can be observed in Eq. (8). Direct comparison between Eq. (8) and the classical solution of LSC presented in Moritz (1980) justifies this statement.

When both input and output are known, the method is focused on the optimal estimation of the transfer function between the input and the output signals (Bendat and Piersol, 1986). In gravity-field-related applications, the output signals are unknown. The fundamental difficulty of the method in the current application is the estimation of the input–output PSD, when the output signal is unknown. In this specific case, the evaluation of the input–output PSD matrix is possible only if the input noise PSD matrix is known. Then, $\mathbf{P_{xy}}$ can be computed by

$$\mathbf{P_{xy}} = \mathbf{H_{xy}}\mathbf{P_{yy}} = \mathbf{H_{xy}}(\mathbf{P}_{\mathbf{y_o y_o}} - \mathbf{P_{mm}}) \tag{9}$$

where $\mathbf{H_{xy}}$ is the transfer function matrix which connects the pure input and output signals. For example, if gravity anomalies are chosen as the input signals, and the geoid as the output signal, then, theoretically, $H_{N\Delta g}$ is nothing other than the Stokes operator in the frequency domain. Using Eq. (9), the final solution of Eq. (8) is given by

$$\begin{aligned}\mathbf{X_o} &= \mathbf{H_{x_o y_o}} \mathbf{Y_o} = \mathbf{H_{xy}}(\mathbf{P_{y_o y_o}} - \mathbf{P_{mm}})\mathbf{P}^{-1}_{\mathbf{y_o y_o}}(\mathbf{Y} + \mathbf{M}) \\ &= \mathbf{H_{xy}}\mathbf{Y} - (\mathbf{H_{xy}}\mathbf{P_{mm}}[\mathbf{P_{yy}} + \mathbf{P_{mm}}]^{-1}(\mathbf{Y} + \mathbf{M}) - \mathbf{H_{xy}}\mathbf{M}) \\ &= \mathbf{X} - \mathbf{E} \end{aligned} \tag{10}$$

According to Eq. (10) it is clear that for the existence of the final solution, the input error PSD matrix $\mathbf{P_{mm}}$ must be known. This is the fundamental difficulty with the frequency domain solution (Sideris 1996). In practice, only the variances of the measurements are known and not the errors themselves. Since the error variances change from point to point, we are dealing with non-stationary noise. The simply algebraic relations in the frequency domain become complicated integral equations when the stationarity assumption is eliminated. This problem is discussed in detail in Sansò and Sideris (1997).

Nevertheless, the advantages of the IOST are indisputable. The spectral character of the method contributes to the fast and efficient handling of large amounts of data. New heterogeneous data can be combined using this technique (e.g. altimetric, airborne, marine, and terrestrial data). Input (stationary) errors can be easily propagated into the results. Proper modification of the transfer function matrix can be achieved in order to minimize the noise-to-signal ratio. In this manner, the input noise is filtered out and error estimates for the predicted results are provided. MIMOS system results are efficiently calculated by computer algorithms due to the smaller matrix dimensions in comparison to space domain techniques, such as LS collocation. In addition, all matrix computations are evaluated in the frequency domain with the convenient matrix division (frequency-by-frequency division), rather than the complicated matrix inversion in the space domain.

2.2 QSST estimation and input data filtering model

The model used in this application is a MIMOS with input data SSHs from the previous-decade altimetric missions of ERS1, ERS2, and T/P, and marine gravity data collected by shipborne gravimetry. The results of the present application are the QSST signal and filtered input data. The number of input SSHs is dependent upon the data availability in the specific time period. For example, for the year 1998, only SSHs from TOPEX/POSEIDON (T/P) and ERS2 can be used as inputs. The model in the case of three input (two SSHs) and four output signals is depicted in Fig. 2, where S_{E1} is the spectrum of the ERS1 signal SSHs, $S_{T/P}$ is the spectrum of the T/P SSHs, DG (ΔG in the equations) is the spectrum of the marine gravity anomalies and T is the output QSST signal.

The optimal transfer function matrix and the final solution in matrix notation are as follows:

$$\mathbf{H_{x_o y_o}} = \begin{bmatrix} H_{T_o S_{E1o}} & H_{T_o S_{T/Po}} & H_{T_o \Delta Go} \\ H_{E1_o S_{E1o}} & H_{E1_o S_{T/Po}} & H_{E1_o \Delta Go} \\ H_{T/P_o S_{E1o}} & H_{T/P_o S_{T/Po}} & H_{T/P_o \Delta Go} \\ H_{\Delta G'_o S_{E1o}} & H_{\Delta G'_o S_{T/Po}} & H_{\Delta G'_o \Delta Go} \end{bmatrix} \tag{11}$$

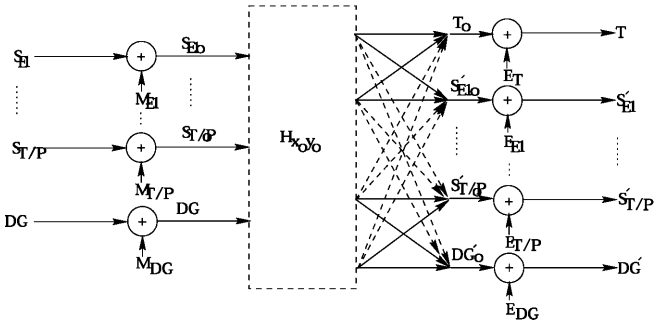

Fig. 2. QSST estimation and filter input data system

$$\begin{bmatrix} T_o \\ E1_o \\ T/P_o \\ \Delta G'_o \end{bmatrix} = \mathbf{H_{x_o y_o}} \begin{bmatrix} S_{E1o} \\ S_{T/Po} \\ \Delta Go \end{bmatrix} \tag{12}$$

The input–output signal PSD can be computed as described in the previous section. In particular, for the case of QSST output and input SSHs from ERS1 and T/P satellites, the equations for the PSD determination are as follows (see e.g. Andritsanos and Tziavos 1999 or Andritsanos et al. 1999):

$$\begin{aligned} T &= S_{\text{mean}} - N = \frac{S_{E1} + S_{T/P}}{2} - N \\ \Rightarrow P_{S_{E1}T} &= S^*_{E1} T = \frac{S^*_{E1} S_{E1} + S^*_{E1} S_{T/P}}{2} - S^*_{E1} N \\ \Rightarrow P_{S_{E1}T} &= \frac{P_{S_{E1}S_{E1}} + P_{S_{E1}S_{T/P}}}{2} - \frac{1}{2\pi\gamma} L_N P_{E1\Delta g} \end{aligned} \tag{13}$$

where γ is the normal gravity and L_N is the Stokes kernel which can be computed directly in the frequency domain with the analytical expression

$$L_N = \frac{1}{\sqrt{u^2 + v^2}} = \frac{1}{q} \tag{14}$$

or, preferably, can be evaluated through the Fourier transform of the kernel in the space domain

$$L_N = \mathbf{F}\{l_N\} = \mathbf{F}\left\{\frac{1}{\sqrt{x^2 + y^2}}\right\} \tag{15}$$

where u and v are the frequencies corresponding to the space domain coordinates x and y. More on the Stokes kernel and its expression in analytical, discrete, planar, or spherical form can be found in Schwarz et al. (1990) and Tziavos (1993). It should be noted that the data introduced to the PSD computations are referenced to a global geopotential model. The derivation of Eq. (13) is possible after the substitution of the unknown geoid signal using Stokes' formula in planar approximation. The cross-PSDs between the other input signals and the QSST signal are estimated following similar procedures

$$P_{S_{T/P}T} = \frac{P_{S_{T/P}S_{E1}} + P_{S_{T/P}S_{T/P}}}{2} - \frac{1}{2\pi\gamma} L_N P_{S_{T/P}\Delta g} \tag{16}$$

$$P_{\Delta gT} = \frac{P_{\Delta gS_{E1}} + P_{\Delta gS_{T/P}}}{2} - \frac{1}{2\pi\gamma} L_N P_{\Delta g \Delta g} \tag{17}$$

In the above equations all related quantities are computed from the input signals. In a simulation study, signals and noises are known quantities and the computations are straightforward. In the present study, a special treatment of the repeated altimetric information is used for the signal and error PSD estimation.

2.3 Signal and error PSD/covariance computation

The repeated altimetric tracks provide a multiple sample configuration of the area under consideration. Using this information a PSD estimation is possible. Following Sailor (1994), we can write for a repeated track analysis

$$h_i = h + \Delta\zeta_i + n_i \tag{18}$$

where h_i is the observed SSH, $i = 1, \ldots, k+1$ is the number of repeated tracks, h is the time-invariant part of the altimetric observation equation (marine geoid and QSST), $\Delta\zeta_i$ is the time-variant part of the SST, and n_i is the altimetric observation noise. The observed SSHs are assumed to be corrected for environmental, geophysical and orbit errors as described in various publications; see, for example, Rowlands (1981), Cheney et al. (1987), Engelis (1987a), Schrama (1989), Denker (1990), Knudsen (1992), AVISO – Altimetrie (1996), Koblinsky et al. (1999). If the deviations from the QSST, $\Delta\zeta_i$, are assumed to follow a random distribution and no correlation exists between $\Delta\zeta_i$ and n_i, then a new random variable e_i can be assigned by

$$\Delta\zeta_i + n_i = e_i \tag{19}$$

This new variable contains the statistical information of the observation noise, as well as the assumed random time-variant part of the SST. We should note that this assumption is not exactly valid in the case of slow-moving oceanographic features (Sailor 1994). In such cases, an oceanographic feature that moves very slowly could be confused with the oceanic geoid signal. Transforming in the frequency domain and subtracting each observation equation from its previous one yields the following set of k difference observations:

$$H_i - H_{i+1} = E_i - E_{i+1} \quad i = 1, \ldots, k \tag{20}$$

The input error PSD can be computed using the complex conjugate form of the previous equation, applying multiplication and assuming no correlation between the input errors

$$k(P_{e_k e_k} + P_{e_{k+1} e_{k+1}}) = 2k\bar{P}_{ee} = \sum_{i=1}^{k} (H_k - H_{k+1})^* (H_k - H_{k+1})$$

$$\Rightarrow \bar{P}_{ee} = \frac{1}{2k} \sum_{i=1}^{k} P_{h_i - h_{i+1}} \tag{21}$$

Using Eq. (21) the input noise PSD can be estimated directly from the observation equations and introduced into the MIMOS. The average error PSD derived by Eq. (21) describes the mean statistical behavior of the error during the time considered. An average of the observations in the specific time interval yields the estimation of the mean observed PSD $\bar{P}_{h_o h_o}$.

Special care is needed in the signal PSD computation. Subtraction of the mean error PSD from the mean observation PSD computed above is not justified since, in the real world, none of the assumptions made in Sect. 2.1 is valid

$$\bar{P}_{h_o h_o} - \bar{P}_{ee} = P_{hh} + P_{he} + P_{eh}, \quad P_{he}, P_{eh} \neq 0 \tag{22}$$

The estimation of the mean signal PSD can be derived by an adequate summation of Eq. (18) using the results of Eq. (21) as follows:

$$H_i + H_{i+1} = 2H + E_i + E_{i+1} \quad i = 1, \ldots, k$$

$$\Rightarrow \sum_{i=1}^{k} P_{h_i + h_{i+1}} = 4k\bar{P}_{hh} + 2k\bar{P}_{ee}$$

$$\Rightarrow \bar{P}_{hh} = \frac{1}{4k} \sum_{i=1}^{k} \left(P_{h_i + h_{i+1}} - P_{h_i - h_{i+1}} \right) \tag{23}$$

Using Eqs. (21) and (23) and the mean observations derived in the considered time interval, an estimation of a mean SST during this period is possible. The deviations from a mean SST are eliminated due to the import of the time-variant part into the error, the use of mean observations, and the average signal PSD. Therefore, the average PSD and data information, when introduced to a MIMOS, yields an estimation of QSST.

3 Test data description and preprocessing

A test area located in the Labrador Sea was selected for numerical experiments based on real altimetric and marine gravity data. The bounds of the test area are $45.05^\circ \leq \phi \leq 55.00^\circ$ and $-55.00^\circ \leq \lambda \leq -45.10^\circ$. This area was selected due to the availability of point shipborne gravity anomalies and its importance for oceanography – the Labrador current is present in this area.

3.1 The satellite altimetry data

AVISO's CD-ROMs containing SSH information were used in this study. This data is corrected for all environmental, geophysical and orbital errors and has passed a robust validation procedure; see AVISO – Altimetrie (1996). Data from the six years of T/P (1992–1998), from the complete mission of ERS1 and its follow-on mission of ERS2 was used. Both AVISO's corrected SSHs (CORSSH) and sea level anomalies (SLA) CD-ROMs were utilized for the yearly-mean signal and error PSD computation, as well as the QSST approximation; see AVISO – Corrected Sea Surface Heights (1997) and AVISO – Sea Level Anomalies (1997). The altimetric observations were classified with respect to the provided Modified Julian Date in specific

directories denoted each year. The start date was 1 January 1993 and the end date was 31 December 1998. The annual periods and the satellite data used in the specific time interval are presented in Table 1.

3.2 Shipborne gravity data

A total of 84 169 point gravity anomalies derived by shipborne gravimetry are available in the test area (Fig. 3). Unfortunately, no information about either the measurement distributions by cruise, or the date the measurements were made, is provided. This is required in order to perform a multiple sample PSD computation. A study on the error covariance behavior in various areas around Europe was recently presented by Behrend (1999), based on the availability of cruise date information. The generation of a multiple sample field can yield an error PSD estimation for the marine gravity data.

3.3 Preprocessing of marine measurements

The contribution of the global geopotential model EGM96 (Lemoine et al. 1998) was computed and subtracted from the point gravity anomalies. The construction of a grid with a spacing of $3' \times 6'$ followed. The final grid was 200×100 elements, and the statistics are presented in Table 2. Due to the absence of error information, simulated Gaussian noise was generated with 5-mGal standard deviation. The statistics of the input noise field are also presented in Table 2.

3.4 Preprocessing of SSH observations

The SSH observations were classified as described in Sect. 3.1. For each time interval the total number of observations was collected for the specific satellite. This was the case for both CORSSHs and SLAs which were used for the error PSD approximation. Finally, the mean observations for each year were computed by applying the generic mapping tools (GMT) routine *blockmean* (Wessel and Smith 1995) to the total number of annual SSHs in order to avoid aliasing of short wavelengths. The result was a mean observation field, from which the contribution of the global geopotential model EGM96 was subtracted, followed by a gridding procedure.

Table 1. Time periods of the altimetric data

Time interval	Satellite data
1/1/1993–12/31/1993	ERS1-phase C, T/P
1/1/1994–12/31/1994	ERS1-GM, T/P
1/1/1995–12/31/1995	ERS1-phase G, ERS2-phase A, T/P
1/1/1996–12/31/1996	ERS1-phase G, ERS2-phase A, T/P
1/1/1997–12/31/1997	ERS2-phase A, T/P
1/1/1998–12/31/1998	ERS2-phase A, T/P

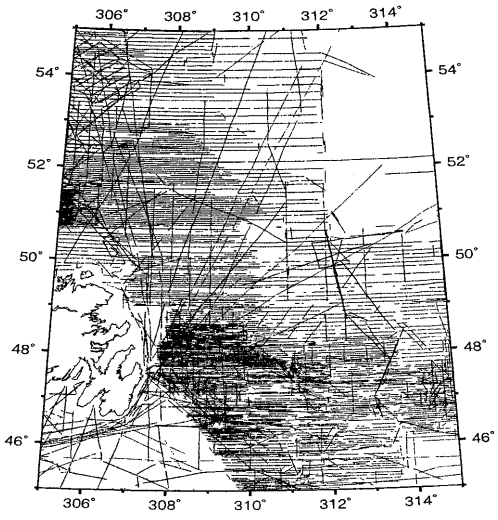

Fig. 3. Marine gravity anomaly data distribution

Table 2. Gravity anomaly observations and noise statistics

Type (mGal)	Max	Min	Mean	RMS	SD
Signal	88.115	−54.968	−2.177	11.174	±10.960
Noise	22.144	−21.963	−0.026	5.023	± 5.023

4 Discussion of numerical results

4.1 Error and signal PSD/covariance estimation

Different strategies were followed for the signal and error PSD computations. In the case of error PSD approximation, two methods were followed. The first one was based on CORSSH processing. The CORSSH observations reduced to the mean sea surface (MSS) given by AVISO (AVISO – Corrected Sea Surface Heights 1997) were used. These observations are given in a 1/s time interval and they do not coincide exactly between successive cycles. In this case, the gridding procedure was unavoidable as a first step, in order to have consistent successive information. A grid of resolution $3' \times 6'$ was constructed in order to be consistent with the marine data. A special arrangement of the ERS1-GM data was made in order to have a multiple sample configuration. Each of the two 168-day cycles is divided in AVISO's CD-ROM into subcycles, with spatial resolution approximately the same as in the ERM configuration, and the gridding procedure was applied to the data of each subcycle. The reduction was performed in order to smooth the data for the gridding procedure and to minimize aliasing in the spectral method. This reduction did not affect the error PSD computation since the MSS cancels out when forming the differences in Eq. (21). A further aliasing minimization technique was used, applying GMT's routine *blockmean* to obtain the average in the specified grid cells. Various gridding techniques were applied, including the GRAVSOFT program *geogrid* (Tscherning et al.

1992) with the weighted means and the collocation-kriging option using the five nearest points for the prediction; and GMT's *surface* routine, which performs gridding with continuous curvature splines in tension (Smith and Wessel 1990). The latter gridding technique was finally selected due to the small discrepancies between the original data and the resulting grid statistics. The collocation-kriging technique gave a smoother field, although far from the original data statistics. A thorough study on the gridding procedures in altimetric and marine data was presented by Kirby (1996), where different interpolation kernels were tested using simulation data analysis. The final result was one-grid-per-cycle files with values in the specific cells. After obtaining the multiple grid information the differences between each cycle grid and the subsequent one were computed. The final mean error PSD approximation for each year was calculated using Eq. (21).

The second method for the error PSD computation was based on SLA files. SLAs are the differences from the MSS, computed at specific common locations for every cycle. For a given track and for each cycle, corrected data are resampled every 7 km using a cubic spline (AVISO – Sea Level Anomalies 1997). In this case, the differences were formed prior to the gridding procedure in order to minimize the error as much as possible in the final estimation. The differences were computed only in locations where there exist values for both successive cycles. The final mean error PSD approximation was computed by Eq. (21). A mean error PSD computation for the data of the ERS1 geodetic mission was not possible using this method since no exact repeat information is available at specific locations.

The computation of the mean error covariances for each year and each satellite followed. The computation was based on the inverse correlogram approach, where the covariance is estimated by the inverse fast Fourier transform (FFT) of the mean error PSD as

$$C_{ee} = \mathbf{F}^{-1}\{P_{ee}\} \tag{24}$$

The resulting variances are given in Table 3.

It is noticeable that the error variance is greater in the first than in the second method. This difference can be attributed to the a priori gridding procedure. As previously mentioned, the *surface* routine used for the grid construction gave the best results with respect to the original point data statistics. Nevertheless, in case of big gaps in the data coverage, the resulting grid was smoother than a field with full coverage. Using the second method (SLA values), although the gridding was limited to the final step just before the PSD estimation procedure, many gaps resulted due to the lack of common data in successive files.

Table 3 shows that T/P has the smallest variances compared with the other satellites. This fact can be partly attributed to the high accuracy of the T/P data, but mainly to the different resolution with respect to the ERS configuration. The lower resolution of the T/P data results in further smoothing in the gridding procedure

Table 3. Computed variances for each satellite and each year. Values in cm^2

Satellite and year	CORSSH case	SLA case
ERS1-C 1993	47.294	35.890
T/P 1993	32.573	27.704
ERS1-GM 1994	33.280	–
T/P 1994	30.085	23.601
ERS1-G 1995	33.579	34.356
ERS2-A 1995	34.677	32.823
T/P 1995	28.738	26.175
ERS1-G 1996	42.465	33.305
ERS2-A 1996	44.134	34.482
T/P 1996	23.956	22.605
ERS2-A 1997	45.784	34.661
T/P 1997	27.498	25.324
ERS2-A 1998	44.831	31.510
T/P 1998	21.919	20.457

and a lower estimate of the error variance. In Figs. 4 and 5, the mean error 2-D covariance, as well as the averaged-over-azimuth 1-D empirical and analytical representations for the year 1998 of the T/P satellite are depicted. The 2-D covariances were computed using the afore mentioned methods for the error PSD approximation and the inverse FFT. A procedure for obtaining the average over the azimuth was applied and an exponential analytical model was used to fit the empirical values.

The SLA estimation procedure resulted in a smoother covariance structure than the CORSSH method due to the different gridding process used.

The fitted analytical error covariance expressions for the 1998 T/P data are as follows:

$$C_{\mathrm{CORSSH}} = 20.852 \cdot \mathrm{e}^{-0.746 \cdot \psi} \tag{25}$$

$$C_{\mathrm{SLA}} = 19.326 \cdot \mathrm{e}^{-0.606 \cdot \psi} \tag{26}$$

In the case of signal PSD computation, the contribution of EGM96 was subtracted in order to smooth the field and to reach consistency with the gravity anomaly observations. An aliasing minimization technique was applied by GMT's routine *blockmean*. The gridding of

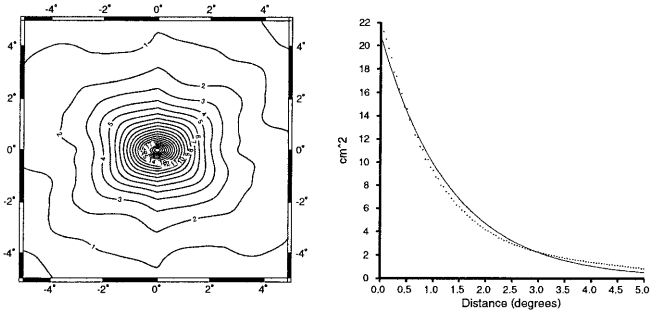

Fig. 4. 2-D error covariance and its 1-D averaged-over-azimuth representation for the 1998 T/P SSHs using the CORSSH method. *Points*: empirical values; *solid line*: analytical expression based on $C = a \cdot \exp(-b\psi)$ model. Contour interval 1 cm^2

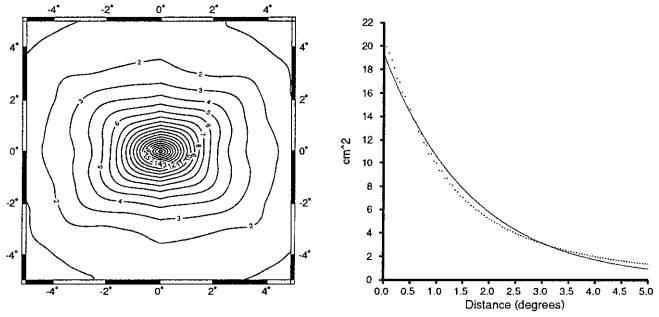

Fig. 5. 2-D error covariance and its 1-D averaged-over-azimuth representation for the 1998 T/P SSHs using the SLA method. *Points*: empirical values; *solid line*: analytical expression based on $C = a \cdot \exp(-b\psi)$ model. Contour interval 1 cm^2

the data followed, using GMT's *surface* routine. Equation (23) was used for the mean signal PSD computation for each year.

A general script was created for an automated computational procedure and for an estimation of the time needed in order for the application to be integrated. The script uses GMT's *blockmean*, *surface*, and *grd2xyz* routines, GRAVSOFT's *harmexp*, and two programs (*noisecomp.f* and *signalcomp.f*) written in Fortran by the authors for the mean signal and error PSD computation. The script was executed on a PC with a Pentium III processor at 450 MHz under the Linux Operating System (kernel 2.2.9). The total computation time was 9 hours 29 minutes and 33 seconds.

The estimation of the input error PSD, as described in the present section, is a critical step in the QSST estimation because valuable information on the statistical behavior of the input error can be extracted. Additionally, the error covariance estimation for each satellite on the specific date can provide interesting conclusions about the oceanic variability.

4.2 QSST estimation

The annual mean signal and error PSD, as well as the annual mean observation field, computed in the previous section, were introduced to the MIMOS. A general program (*ioprog4.f*) written in Fortran and based on the theoretical background of Sect. 2.1 was used for the QSST estimation and the input data filtering. As previously mentioned, the input error PSD matrix must be known in order to estimate the optimal impulse response function matrix. The input error PSD for the SSHs was computed following the methodology presented in Sect. 2.3. In the case of the gravity anomaly field, a simulated noise field was assumed. The elements of the noise field followed the Gaussian distribution with a standard deviation of 5 mGal. It is worth mentioning that, using the cruise date information, the computation of the error PSD is possible following a similar procedure to that of the SSHs.

The computations were performed firstly with PSDs derived by the CORSSH method and secondly with PSDs derived by the SLA method. The QSST mean annual estimates by the CORSSH method are presented in Table 4. The differences between the two solutions are given in Table 5.

Note that the maximum values of the QSST estimates are caused by the presence of land masses in the test area. The differences in the QSST computation due to the adopted PSD estimation method (CORSSH, SLA) are minor, as shown in Table 5. The QSST estimation for the year 1996 is depicted in Fig. 6, where some short-wavelength features are present. These features can be attributed to the marine gravity data gaps and the inappropriate error modeling for the shipborne gravity anomalies; see, for example, discussion by Engelis (1985). The dense contour intervals in the lower left part of the figure are caused by the presence of land masses.

In order to validate our solution two comparisons with pure oceanographic-derived SST estimates followed. A solution comparable to the global pure oceanographic spherical harmonic analysis of Levitus SST (Levitus 1982) performed by Engelis (1987a) was obtained with the application of a Gaussian low-pass filter to the QSST field. All wavelengths smaller than 10° (1111 km – harmonic degree 36) were eliminated. This choice was made in order to keep the frequency content comparable to Engelis' solution. The resulted QSST field is depicted in Fig. 7.

Comparing Fig. 7 with Engelis' Fig. 14 (Engelis 1987a), similar features can be identified. The overall behavior of the filtered field is approximately the same as in the purely oceanographic-derived solution. A bias between the two solutions can be detected. This bias can be explained by the difference between the QSST estimated by MIMOST and the complete magnitude of the SST field expressed by Engelis' expansion. The complete SST field contains the time-variant part of the SST which is absent in the QSST estimate. In particular, in the test area, the Labrador current and the edge of the Gulf Stream are present and affect the local solution. Another reasonable explanation for the

Table 4. QSST annual estimation by MIMOST. Values in m

Year	Max	Min	Mean	RMS	SD
1993	1.795	−0.533	0.379	0.533	±0.374
1994	1.721	−0.585	0.373	0.527	±0.373
1995	1.736	−0.544	0.372	0.518	±0.361
1996	1.766	−0.558	0.388	0.533	±0.365
1997	1.880	−0.518	0.393	0.551	±0.387
1998	1.914	−0.507	0.388	0.542	±0.379

Table 5. Differences in the QSST estimation using input error PSD computed by CORSSH and SLA methods. Values in m

Year	Max	Min	Mean	RMS	SD
1993	0.014	−0.012	0.001	0.003	±0.003
1994	0.004	−0.004	0.001	0.001	±0.001
1995	0.008	−0.009	0.000	0.002	±0.002
1996	0.010	−0.016	0.000	0.003	±0.003
1997	0.011	−0.017	0.000	0.003	±0.003
1998	0.018	−0.031	0.000	0.004	±0.004

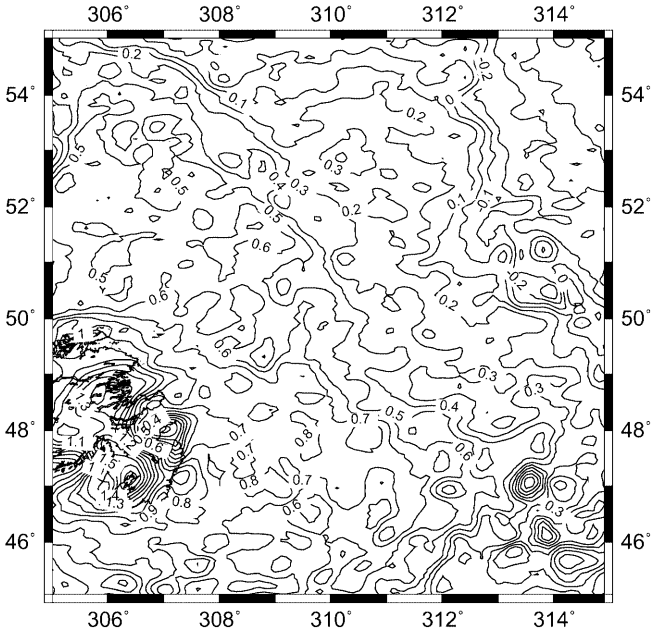

Fig. 6. QSST estimation for the year 1996. Contour interval 0.1 m

presence of this bias is the well-known weakness of the oceanographic solution: an equi-pressure surface of 2250 mb was used as an equipotential surface for the reference of the oceanographic solution (Engelis 1985). Such a surface seems to approximate most closely a level surface on a global basis; see, for example, Montgomery (1969). The uncertainty of this choice can be lead to a bias datum inconsistency. Of course, the time period between the two independently derived solutions is different and some inconsistencies between the results can be attributed to this time difference.

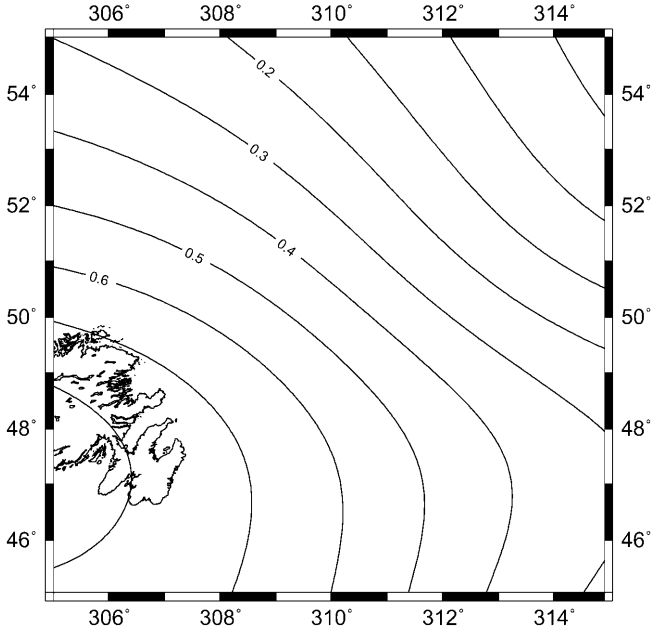

Fig. 7. Low-pass-filtered QSST estimation for the year 1996. Contour interval 0.1 m

Finally, the datum of the marine gravity anomalies, in combination with the problematic measurement environment of shipborne gravimetry, can introduce another source of errors; see, for example, Talwani (1966), Prince and Forsyth (1984), and Wessel and Watts (1988).

Additionally, a numerical comparison between our solution and the global spherical harmonic solution presented in Pavlis et al. (1998) was performed. The spherical harmonic SST coefficients were derived from an LS fit to the output of the parallel ocean circulation model (POCM-4B) (Stammer et al. 1996), to a maximum degree 30. The POCM-4B output used was temporally averaged for the years 1993 and 1994 (T/P cycles 11 to 84) (Pavlis et al. 1998). A low-pass filter was applied to the 1994 QSST MIMOS solution with a cut-off wavelength of 1333.333 km (harmonic degree 30). The two solutions were compared before and after a bias and tilt fit and the results are presented in Table 6. A four-parameter model was used for the bias and tilt fit.

As can be seen from Table 6, the agreement between our local altimetric–gravimetric based solution and the global pure oceanographic spherical harmonic solution is of the order of 7.3 cm standard deviation (SD), after a bias and tilt parametric fit. The bias and tilt can be attributed to the same reasons as described in the previous comparison. The different methodology used for each solution (global spherical harmonic SST solution–local MIMOS QSST estimation), as well as the absence of the time-variant part of the SST in our solution, are responsible for the residual long-wavelength patterns that can be identified in Fig. 8. It is worth mentioning that these comparisons were performed in order to show the consistency between two QSST estimation methods and to mention the methodological differences. The SD of the differences provides only a magnitude of the external accuracy since it is not possible to make comparisons in such small blocks of signal (10-degree blocks smoothed over 10 degrees). Some comparisons between a global harmonic solution and a local filtering technique were presented in Engelis (1983), where the conceptual differences of the methodologies used were explained.

In order to verify the quasi-stationary (time-invariant) character of our estimation, the differences with respect to the QSST of 1993 were computed. The mean values of the differences, both for the CORSSH and for the SLA PSD estimation methods, are presented in Fig. 9.

It can be seen that the difference in the mean value fluctuates around zero in the time period under consideration. A similar diagram is depicted in Fig. 10 for the standard deviations of the differences with respect to the

Table 6. Differences between the filtered 1994 QSST solution and the global SST harmonic solution of POCM-4B. Values in m

	Max	Min	Mean	SD
Before bias + tilt fit	−0.957	−1.380	−1.258	±0.092
After bias + tilt fit	0.281	−0.152	0.000	±0.073

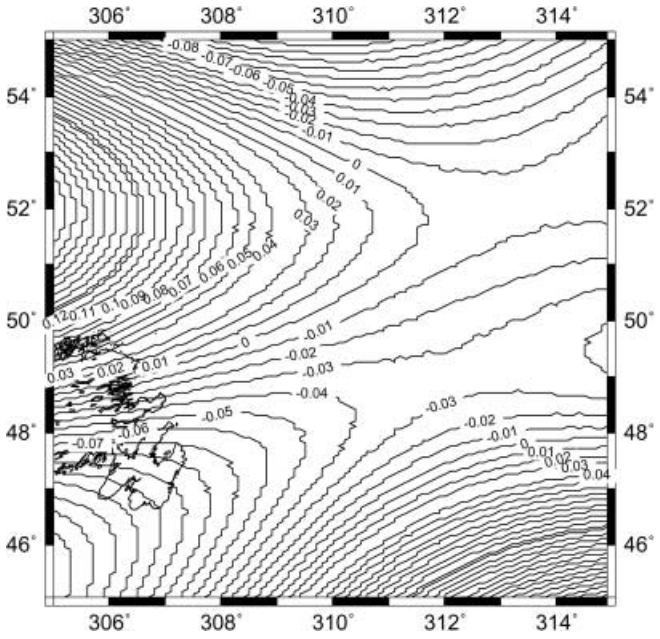

Fig. 8. Differences between the global spherical harmonic solution and the local MIMOS QSST estimation for 1994 after a bias + tilt fit. Contour interval 0.01 m

1993 QSST. The standard deviations present an expected stability within MIMOST accuracy. A longer study period is needed in order to confirm the aforementioned statements.

5 Summary, conclusions and recommendations

The application of the MIMOST to the QSST estimation was presented. SSHs from recent altimetric missions and marine gravity anomalies were optimally combined and the repeat tracks of the exact repeat mission (ERM) configuration were used for the input error PSD computations. The CORSSH- and SLA-based methods for the input error and signal PSD approximation were presented. The derived PSDs were compared with each other and used in the QSST estimation through the MIMOS.

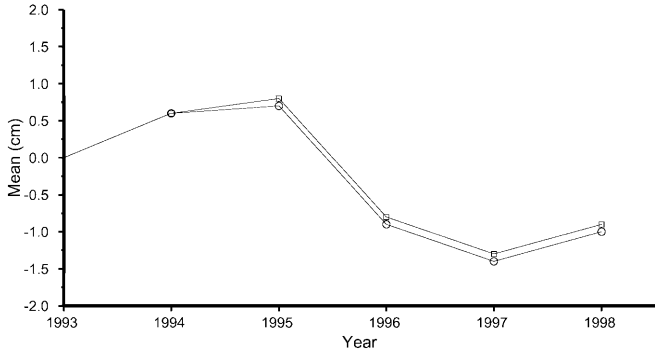

Fig. 9. Differences in the mean of the QSST estimations with respect to 1993. Values in cm. *Squares*: CORSSH method; *circles*: SLA method

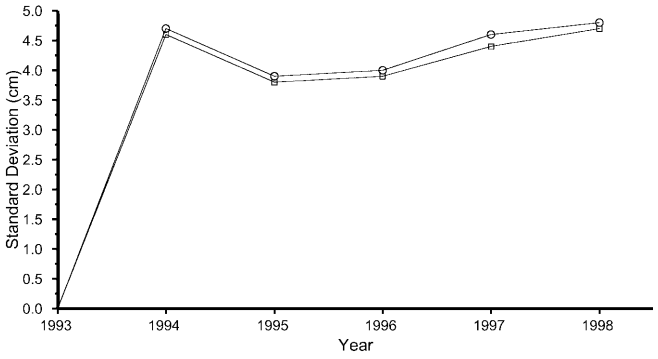

Fig. 10. Differences in the SD of the QSST estimations with respect to 1993. Values in cm. *Squares*: CORSSH method; *circles*: SLA method

Input error PSDs computed by the SLA method showed a smoother behavior compared with the one computed by the CORSSH method. This was caused by the different procedure in the estimation: a gridding procedure was the first step in the CORSSH method, while in the SLA method the gridding was applied only before the PSD estimation. Nevertheless, due to the low sensitivity of the MIMOST to the input error, the apparent differences affected the QSST estimation in only a minor way. The time-invariant character of the estimation was verified considering a time period of 6 years. This period is not adequate for annual sea level variation studies and a longer interval is needed. Comparisons with the global individual oceanographic SST solution of Levitus, expanded in spherical harmonics by Engelis, as well as the global spherical harmonic expansion of POCM-4B, showed interesting similarities in the basic features of SST. An apparent bias was attributed to datum inconsistencies between solutions.

The extraction of the time-variant part of the SST from the input error PSD is the basic topic of our future work. In the case where the time-variant SST is part of the system signal, the continuous monitoring of local areas of interest is possible since the estimation of the complete SST component is the MIMOS result. The automated procedure described in Sect. 4.1 will contribute to this goal. The combined estimation of the SST using both oceanographic and geodetic data is another prospective research field. Following the methodology presented, error models for both altimetric and marine data could be computed in local and regional areas. The gridding disadvantage in the PSD estimation could be confronted by special treatment in the FFT algorithm, due to the characteristic configuration of the altimetric data. Further research in this area could also yield interesting results in the area of gravity field modeling. Another interesting application is the possible introduction of parametric models such as ARMA (autoregressive moving average) and MA (moving average) [see, for example, analysis in Blais and Vassiliou (1987), Marple (1987) and Kay (1987) for 1-D data and Cadzow and Ogino (1981) for 2-D data] in the PSD estimation of irregularly distributed data, such as shipborne gravity anomalies. Additionally, the advent of the gravity field dedicated missions CHAMP, GRACE, and GOCE

could lead to a more accurate SST estimation due to the availability, the resolution and the improved accuracy of the observed gravity field.

Acknowledgements. This paper was completed while the first author was a visiting scientist at the University of Calgary. The authors would like to thank Dr. N.K. Pavlis for providing the POCM-4B spherical harmonic coefficient set and the respective software to access the coefficient file. The financial assistance provided to the first author by the Hellenic National Scholarship Foundation and by a GEOIDE Network of Centres of Excellence (NCE) project is gratefully acknowledged.

References

Andritsanos VD, Tziavos IN (2000) Estimation of gravity field parameters by a multiple input/output system. Phys Chem Earth 25: 39–46

Andritsanos VD, Sideris MG, Tziavos IN (1999) Sea surface topography estimation by a generalised multiple input/output method. Poster presented at the XXII IUGG General Assembly, Birmingham, 18–30 July

AVISO – Altimetrie (1996) AVISO user handbook – merged TOPEX/POSEIDON products, 3rd edn. AVI-NT-02-101-CN, Toulouse, France

AVISO – Corrected Sea Surface Heights (1997) AVISO user handbook – corrected sea surface heights, 3rd edn. AVI-NT-011-311-CN, Toulouse, France

AVISO – Sea Level Anomalies (1997) AVISO user handbook – sea level anomalies, 2nd edn. AVI-NT-011-312-CN, Toulouse, France

Behrend D (1999) Error covariance functions for marine gravity data in the European seas. Poster presented at the XXII IUGG General Assembly, Birmingham, 18–30 July

Bendat JS, Piersol AG (1986) Random data: analysis and measurement procedures. John Wiley, New York

Blais JAR, Vassiliou AA (1987) Spectral analysis of one-dimensional data sequences. UCSE Rep 30010, University of Calgary, Alberta, Washington, D.C.

Cadzow JA, Ogino K (1981) Two-dimensional spectral estimation. IEEE Trans Acoust Speech Signal Process 29: 396–401

Cheney RE, Doyle NS, Douglas BC, Agreen RW, Miller L, Timmerman EL, McAdoo DC (1987) The complete geosat altimeter GDR handbook. NOAA, US Department of Commerce, Washington, D.C.

Denker H (1990) Radial orbit error reduction and sea surface topography determination using one year of GEOSAT altimeter data. Rep 325, Department of Geodetic Science and Surveying, The Ohio State University, Columbus

Engelis T (1983) Analysis of sea surface topography using SEASAT altimeter data. Rep 343, Department of Geodetic Science and Surveying, The Ohio State University, Columbus

Engelis T (1985) Global circulation for SEASAT altimeter data. Mar Geod 9: 45–69

Engelis T (1987a) Radial orbit error reduction and sea surface topography determination using satellite altimetry. Rep 377, Department of Geodetic Science and Surveying, The Ohio State University, Columbus

Engelis T (1987b) Spherical harmonic expansion of the Levitus sea surface topography. Rep 385, Department of Geodetic Science and Surveying, The Ohio State University, Columbus

Engelis T, Knudsen P (1989) Orbit improvement and determination of the oceanic geoid and topography from 17 days of Seasat data. Manuscr Geod 14: 193–201

Hwang C (1987) Orthonormal function approach for GEOSAT determination of sea surface topography. Mar Geod 18: 245–271

Kay SM (1987) Modern spectral estimation. Prentice-Hall, Englewood Cliffs

Kirby JF (1996) The development and application of a new algorithm for ocean geoid recovery. Dissertation, University of Edinburgh

Knudsen P (1991) Simultaneous estimation of the gravity field and sea surface topography from satellite altimetry data by least-squares collocation. Geophys J Int 104: 307–317

Knudsen P (1992) Altimetry for geodesy and oceanography. In: Kakkuri J (ed) Geodesy and geophysics. Finnish Geodetic Institute, Masala, pp 87–129

Koblinsky CJ, Ray R, Beckley BD, Wang YM, Tsaoussi L, Brenner A, Williamson R (1999) NASA – ocean altimeter pathfinder project report 1: data processing handbook. NASA Tech memorandum 1998-208605, Greenbelt, MD

Lemoine FG, Kenyon SC, Factor JK, Trimmer RG, Pavlis NK, Chinn DS, Cox CM, Klosko SM, Luthcke SB, Torrence MH, Wang YM, Williamson RG, Pavlis EC, Rapp RH, Olson TR (1998) The development of the joint NASA GSFC and NIMA geopotential model EGM96. NASA Tech paper, 1998-206861

Levitus Su (1982) Climatological atlas of the world ocean. Professional paper 13, NOAA, Geophysical Fluid Dynamics Laboratory, Silver Spring, MD

Li J (1996) Detailed marine gravity field determination by combination of heterogeneous data. Master's thesis, UCSE rep 20102, Department of Geomatics Engineering, The University of Calgary, Alberta

Marple S (1987) Digital spectral analysis with applications. Prentice- Hall, Englewood Cliffs

Montgomery RB (1969) Comments on oceanic leveling. Deep Sea Research, Suppl vol 16, pp 147–162

Moritz H (1980) Advanced physical geodesy. Wichmann, Karlsruhe

Pavlis NK, Cox CM, Wang YM, Lemoine FG (1998) Further analyses towards the introduction of ocean circulation model information into geopotential solutions. Presented at the 2nd Joint Meeting of the International Gravity Commission (IGC) and the International Geoid Commission (IGes), Trieste, 7–12 September

Prince RA, Forsyth DW (1984) A simple objective method for minimizing crossover errors in marine gravity data. Geophysics 49: 1070–1083

Rao DB, Steenrod SD, Sanchez BV (1987) A method of calculating the total flow from a given sea surface topography. NASA Tech Memorandum 87799, Greenbelt, MD

Rapp RH, Wang YM, Pavlis NK (1996) Analysis of dynamic ocean topography using TOPEX data and orthonormal functions. J Geophys Res 101: 22 583–22 598

Rowlands D (1981) The adjustment of SEASAT altimeter data on a global basis for geoid and sea surface height determinations. Rep 325, Department of Geodetic Science and Surveying, The Ohio State University, Columbus

Sailor RV (1994) Signal processing techniques. In: Vanicek P, Christon NT (eds) Geoid and its geophysical interpretations. CRC Press, Boca Raton, FL, pp 147–185

Sanchez BV, Cunningham WJ, Pavlis NK (1997) The calculation of the dynamic sea surface topography and the associated flow field from altimetry data: a characteristic function method. J Phys Oceanog 27: 1371–1385

Sanso F, Sideris MG (1997) On the similarities and differences between systems theory and least-squares collocation in physical geodesy, Boll Geod Sci Aff 2: 174–206

Schrama EJO (1989) The role of orbit errors in processing of satellite altimeter data. Rep 33, Publications on Geodesy, New Series, Netherlands Geodetic Commission, Delft

Schwarz KP, Sideris MG, Forsberg R (1990) The use of FFT techniques in physical geodesy. Geophys J Int 100: 485–514

Sideris MG (1996) On the use of heterogeneous noisy data in spectral gravity field modeling methods. J Geod 70: 470–479

Smith WHF, Wessel P (1990) Gridding with continuous curvature splines in tension. Geophysics 55: 293–305

Stammer D, Tokmakian R, Semtner A, Wunsch C (1996) How well does 1/4° global circulation model simulate large-scale oceanic observations? J Geophys Res 101: 25 779–25 812

Tai CK, Wunsch C (1984) An estimate of global absolute dynamic topography. J Phys Oceanog 14: 457–463

Talwani M (1966) Some recent developments in gravity measurements abroad surface ships. In: Orlin H (ed) Gravity anomalies: unsurveyed areas, Geophysical monograph no 9. American Geophysical Union, Washington, DC

Tscherning CC, Knudsen P, Forsberg R (1997) Description of the GRAVSOFT package. Proc 1st Continental Workshop on the Geoid in Europe, Prague, 11–14 May. Published by the Research Institute of Geodesy, Topography and Cartography. In: Holota P, Vermeer M (eds) pp 327–347

Tziavos IN (1993) Numerical considerations FFT methods in gravity field modeling. Rep 188, Wissenschaftliche Arbeiten der Fachrichtung Vermessungswesen, University of Hannover

Tziavos IN, Forsberg R, Sideris MG, Andritsanos VD (1996a) A comparison of satellite altimetry methods for the recovery of gravity field quantities. In: Forsberg R, Feissel M, Dietrich R (eds) Proceedings of the IAG Scientific Assembly Gravity, Geoid, Geodynamics and Antarctica, Rio de Janeiro, 3–9 September, pp 150–155

Tziavos IN, Li J, Sideris MG (1996b) Marine gravity field modeling using non-isotropic a-priori information. In: Sagawa J, Fujimoto H, Okubo S (eds) Proceedings of the IAG Symposium Gravity, Geoid and Marine Geodesy, Tokyo, 30 September–5 October, Springer, Berlin, Heidelberg, New York, pp 400–407

Tziavos IN, Sideris MG, Li J (1996c) Optimal spectral combination of satellite altimetry and marine gravity data. In: Tziavos IN, Vermeer M (eds) Proceedings of the XXI EGS General Assembly 'Techniques for local geoid determination', The Hague, pp 41–56

Tziavos IN, Siders MG, Forsberg R (1998) Combined satellite altimetry and shipborne gravimetry data processing. Mar Geod 21: 299–317

Wessel P, Smith WHF (1995) New version of generic mapping tools released. EOS Trans Am Geophys union 76: 329

Wessel P, Watts AB (1988) On the accuracy of marine gravity measurements. J Geophys Res 93: 393–413

Wu L, Sideris MG (1995) Using multiple input–single output system relationships in post processing of airborne gravity vector data. Proceedings of the Symposium on Airborne Gravity Field Determination, IUGG XXI General Assembly, Boulder, pp 87–94